Vernay, D.G., Favre, F.X. and Smith, I.F.C. "Robust model updating methodology for estimating worst-case load capacity of existing bridges" Journal of Civil Structural Health Monitoring, Vol 8, No 5, 2018, pp773–790 doi:10.1007/s13349-018-0305-4

Robust model-updating methodology for estimating worst-case load capacity of existing bridges

Didier G. Vernay [1,*], François-Xavier Favre [1,2], Ian F.C. Smith [1,2].

[1] ETH Zurich, Future Cities Laboratory, Singapore-ETH Centre, CREATE, Singapore

[2] Swiss Federal Institute of Technology Lausanne (EPFL), Applied Computing and Mechanics Laboratory (IMAC), School of Architecture, Civil and Environmental Engineering (ENAC), Lausanne, Switzerland

* Corresponding author: Didier G. Vernay, Tel.: +65 9221 1622, E-mail: didiervrn@gmail.com

Abstract

High-value infrastructure elements, such as bridges, are typically over-designed. Model-updating techniques are useful for estimating the reserve load capacity (beyond safety factors) of bridges and this improves sustainability through good asset-management decision making. In these approaches, measurement data are used to infer model parameter values that influence behaviour. Several approaches have been proposed for structural model updating. Population approaches, such as Bayesian updating, reflect the intrinsically ambiguous nature of diagnosis as well as a range of uncertainty sources. However, many do not consider bias in model formulations, which results in biased identification of parameter values and subsequent predictions. Also, discrete sampling methods may be too coarse to be able to identify critical parts of the population where worst case reserve capacity is determined. In this paper, a new methodology is proposed to update models of structural systems using measurements. This methodology has been employed to identify the most critical set of parameter values for the bending ultimate limit state (ULS) verification and the serviceability limit state (SLS) verification of an existing reinforced concrete bridge after gaining information from measurements. This methodology is based on the error-domain model falsification approach, in which measurements are used to falsify models rather than calibrate them. Through a full-scale case study, it is shown that the new methodology is able to provide a parameter-value set that is more accurate for ULS and SLS verification than those identified with residual minimization. Furthermore, it is shown that residual minimization (traditional curve fitting) may result in unsafe estimates of reserve capacity.

1. Introduction

Existing structures often have reserve capacity because they have been designed with simple, conservative models. More accurate estimates of real behaviour are needed once infrastructure is in service in order to improve management decisions. For example, when decisions related to either replacement or repair are involved, knowledge of real behaviour may contribute significantly to lowering costs and improving sustainability. Model updating techniques have the potential to improve predictive capability of behavioural models by estimating parameter values using observations. For example, direct measurements, such as non-destructive tests, and indirect measurements, such as measurements of behaviour during load tests, can be used to update a finite-element model (FEM). In this paper, the focus is to update a FEM using measurements of behaviour obtained during static-load tests. This constitutes an inverse problem because parameter values are inferred through comparing predictions of a FEM with measurements. Inverse problems are ambiguous tasks since many sets of parameter values can provide the same prediction at a sensor location (Beven 2006). Such ambiguities are amplified by uncertainties in models and measurements. Modelling errors originate from intentional model simplifications as well as omissions of physical phenomena due to a lack of knowledge (Draper 1995).

The vast majority of model-updating strategies involve minimizing the differences between predictions and measurements to obtained one ‘optimal’ model (Çatbaş, Kijewski-Correa, and Aktan 2013; Mottershead, Link, and Friswell 2011; Spencer Jr. and Cho 2011). Model simplifications and omissions result in systematic biases in model predictions at measurement locations. These model biases, if known, should be accommodated during model calibration. If not, model calibration approaches provide parameter values which compensate epistemic model biases at measurement locations (Atamturktur et al. 2015). Therefore, the ‘optimal’ model obtained with model calibration is unacceptably dependent on sensor locations (and model biases at those locations). Furthermore, prediction using such models is precarious, particularly when extrapolating, yet such activity is unavoidable in asset management.

An alternative strategy is based on the recognition that measurements are more useful when they falsify models rather than calibrate them (Tarantola 2005, 2006). This has led to methodologies for model falsification in areas such as environmental science (Beven 2002) and civil engineering (Raphael and Smith 1998). Error-domain model falsification (EDMF) (Goulet, Kripakaran, and Smith 2010) is one such methodology. In this methodology, threshold bounds are estimated by combining measurement noise and modelling uncertainties at sensor locations. A model instance is a candidate if the differences between measurements and model predictions fall within threshold bounds for each and every measurement location.

Otherwise, the model instance is falsified. In traditional applications of EDMF, the Monte Carlo method or Latin Hypercube Sampling (LHS) was often used to create an initial population of model instances by sampling in the prior parameter domain (Goulet, Kripakaran, and Smith 2010; Pasquier and Smith 2016). Candidate models, obtained after falsification, are then employed to predict reserve capacity. EDMF has been used to estimate the reserve capacity of bridges for the limit state of deflection (Goulet, Kripakaran, and Smith 2010) and for fatigue life (Pasquier et al. 2016). However, sampling methods such as LHS often result in sampling that is too coarse to be able to identify worst-case model-parameter values with reasonable accuracy.

Due to a lack of knowledge, modelling uncertainties of complex systems cannot usually be described with sophisticated probability density functions. Thus, a methodology that only requires the definition of uncertainty bounds is more appropriate for model updating than traditional probabilistic approaches. Probabilistic approaches such as Bayesian model updating (Beck and Au 2002; Beck and Katafygiotis 1998) typically propose the definition of independent zero-mean Gaussian uncertainty distributions. Extensions to this approach include representation of correlations (Simoen et al., 2013). Fuzzy approaches are also employed for uncertainty estimation. In these approaches, fuzzy sets are employed to describe possible model outputs and measurement data. If these sets are overlapping, fuzzy operators such as union or intersection operators can be used to determine the degree of membership of each model (Huang and Teghem 2012; Urbanski and Wąsowski 2003). This approach has been used to detect changes in structural properties in application to damage detection (Sawyer and Rao 2000). However, inputs such as the membership functions between bounds and the definition of fuzzy operators are needed. Information is rarely available to define accurately these inputs. Other approaches to damage detection using artificial neural networks have been used, for example (Neves et al. 2017). However, neural networks implement a form of non-linear regression that is suitable only for interpolation. When weighing asset-management decisions in civil engineering related to repair, replacement and extension of structures, support for extrapolation is needed.

In civil engineering, model-updating strategies that involve sampling the parameter domain using either the Monte Carlo method or LHS are appropriate for performing probabilistic safety verification (Brühwiler et al. 2012). However, little information is explicitly available regarding the likelihood of models given measurements and thus, the predictive distributions used to compute probability of failure are approximate. An alternative, which is employed in this paper, is to determine the most critical set of parameter values after model falsification and use the partial safety factor format for safety verification. This strategy is appropriate for model updating of critical systems where uncertainties are represented by intervals

(threshold bounds). Furthermore, many models are able to explain measurements because of the inverse nature of the task. Of these models, it is of interest to determine the model that provides the worst-case prediction.

Non-linear finite-element analysis (NLFEA) has been used to assess the performance of existing structures at the ultimate limit state. Schlune et al. (2012) concluded that model uncertainties of non-linear finite element analyses need to be higher than those employed in traditional designs based on linear finite element analyses. These uncertainties depend on the failure mode. For instance, it was reported that coefficients of variation for model uncertainty are in the range of 5 to 30% for bending and 15 to 64% for shear (Cervenka 2013). The FEM needs to be validated with field data in order to reduce these uncertainties (Pimentel, Brühwiler, and Figueiras 2014). Additional uncertainty quantification and strategies to improve the modelling of existing structures can be found in (Nishio and al. 2012).

In this paper, a new methodology based on error-domain model falsification is proposed in order to find the most critical set of parameter values for ULS and SLS verification given measurement data. Then, the load capacity is estimated using the most critical set of parameter values obtained for ULS and SLS verification. For SLS verification, a linear finite element analysis is performed using the most critical set of parameter values in order to estimate the load capacity while a non-linear finite element analysis is used to estimate ULS load capacity. Finally, the usefulness of measurements for improving estimations of load capacity at the ULS is evaluated.

In Section 2, the traditional implementation of error-domain model falsification and the new methodology, which is based on EDMF, is described. In Section 3, the case study is presented and results of residual minimization are compared with those of the new methodology for identification and prediction tasks. Finally, Section 4 contains discussion of the results and future work.

2. Methodology

2.1 Background - Error-domain model falsification

Error-domain model falsification has been developed for applications in which measurement noise and modelling errors cannot be described by multivariate probability density functions due to a lack of knowledge related to uncertainties and their correlations.

As in other model-updating approaches, error-domain model falsification involves identifying parameter values $\boldsymbol{\theta} = [\theta_1, \dots, \theta_{n_p}]^T$ of a physics-based model using information from measurements, where n_p is the number of parameters that require identification. Bounds of parameter values are defined using engineering knowledge.

At sensor location x_i, the true behaviour Q_i can be estimated by correcting the prediction of the model $g(x_i, \boldsymbol{\theta})$ with a value of modelling error $\epsilon_{i,g}$. As parameter values and errors cannot be determined deterministically, they are random variables, and the relation between them can be expressed as follows:

$$Q_i = g(x_i, \boldsymbol{\Theta}) + U_{i,g}, \quad \forall i = 1, 2, \dots, n_y \tag{1}$$

where $\boldsymbol{\Theta}$ is a random variable describing $\boldsymbol{\theta}$, $U_{i,g}$ is a random variable describing $\epsilon_{i,g}$ and n_y is the number of sensor locations.

Similarly, the true behaviour can also be approximated by correcting the measurement data y_i with a value of measurement error $\epsilon_{i,y}$, which depends on the sensor accuracy. This relation can be expressed using random variables as follows:

$$Q_i = y_i + U_{i,y}, \quad \forall i = 1, 2, \dots, n_y \tag{2}$$

Where $U_{i,y}$ is a random variable describing $\epsilon_{i,y}$.

By combining Equations 1 and 2, it is deducted that the difference between the prediction of the model and the measurement at location i is equal to the difference between modelling and measurement uncertainties at this location as expressed in the following equation.

$$g(x_i, \boldsymbol{\Theta}) - y_i = U_{i,y} - U_{i,g} = U_{i,c}, \quad \forall i = 1, 2, \dots, n_y \tag{3}$$

where $U_{i,c}$ is the combined uncertainty at location i. In standard implementations of EDMF, the Monte Carlo method is employed to compute the combined uncertainty from estimated distributions of uncertainty sources (modelling and measurement uncertainties).

The most important parameters are identified using a sensitivity analysis. Following the notation in Equations 1-3, an initial model set Ω_k is generated through assigning parameter-value sets $\boldsymbol{\theta}_m$ to a specific model class G_k. In standard implementations of EDMF, the initial set of model instances is generated by Latin Hypercube Sampling.

The model instance defined by the parameter-value set $\boldsymbol{\theta}_m$ is falsified, if for any measurement location $i \in \{1, 2, \dots, n_y\}$ the difference between predicted and measured values is outside the interval defined by the threshold bounds $[T_{i,low};\ T_{i,high}]$. Otherwise, the model instance is a candidate model and satisfies Equation (4).

$$T_{i,low} \leq\ g(x_i, \boldsymbol{\theta}) - y_i \leq\ T_{i,high}\ , \forall i \tag{4}$$

Thresholds bounds are calculated using the combined uncertainty and by using a confidence level ϕ_d. In practice, a value of 95% is used for the confidence level. The Sidak correction (Šidák 1967) is used to correct the confidence level by taking into account that many measurements are used simultaneously to falsify models. This leads to determination of consistent threshold bounds for each measurement location. Threshold bounds $[T_{i,low}; T_{i,high}]$ of combined uncertainties are obtained by finding the tightest bounds in the following equation.

$$\phi_d{}^{1/n_y} = \int_{U_{i,c} = T_{i,low}}^{U_{i,c} = T_{i,high}} f_{U_{i,c}}(U_{i,c}) dU_{i,c}, \qquad \forall i \in \{1, 2, \dots, n_y\} \tag{5}$$

Where $f_{U_{i,c}}(U_{i,c})$ is the probability density function of the continuous random variable, $U_{i,c}$.

All model instances that have been falsified are assigned a probability of 0. As little information is available regarding modelling uncertainties, the remaining candidate models are assigned a constant probability of $\frac{1}{n_{cand}}$ where n_{cand} is the number of candidate models.

Finally, if the candidate model set is not empty, the predictive distribution at unmeasured locations x_j can be obtained according to Equation (6).

$$Q_j = \mathrm{g}(x_j, \boldsymbol{\Theta}^*) + U_{j,g} \tag{6}$$

where $g(x_j, \boldsymbol{\Theta}^*)$ is a distribution of predictions at location x_j using the parameter-values sets $\boldsymbol{\Theta}^*$ that have been identified $\boldsymbol{\Theta}^* = \{\boldsymbol{\theta} | \boldsymbol{\theta} \in \Omega^*\}$ and $U_{j,g}$ is a random variable describing the modelling error at location x_j. In previous case studies, prediction bounds at unmeasured locations have been calculated by taking the 95% confidence interval of the predictive distribution obtained in Equation (6) (Pasquier and Smith 2015).

2.2 New methodology compatible with EDMF

A new methodology, based on constrained optimization method and compatible with error-domain model falsification, is developed below. In this methodology, constrained optimization is used to find the most critical set of parameter values for a specific limit state given constraints from measurement data. This set provides predictions that fall inside threshold bounds computed using Equation (5).

The most critical set of parameter values is obtained through maximizing an objective function $f(\boldsymbol{\theta})$ under constraints. The objective function to be maximized is the effect of traffic loads (taken from codes) on bridge components needed for ULS or SLS verification. Constraints are provided by prior knowledge of parameter values (which are bounded) and by measurement data using Equation (4).

Figure 1 presents an illustrative example of constrained optimization with two parameters and using one sensor data point y_1 for falsification. In this illustration, $g(x_1, \theta_1, \theta_2)$ is the predicted value of the finite element model used to simulate the behaviour of the bridge under test loads at the sensor location x_1 and the objective function $f(\theta_1, \theta_2)$ is the predicted value of the finite element model under the loads of the codes needed for ULS or SLS verification. The dark lines are isolines of the objective function. The horizontal and vertical dashed lines represent the bounds of parameter values (first set of constraints). The curved dashed lines corresponding to $g(x_1, \theta_1, \theta_2) - y_1 < T_{1,low}$ and $g(x_1, \theta_1, \theta_2) - y_1 > T_{1,high}$ represent the second set of constraints, provided by the measurement y_1 (Equation 4). The resulting white area is the feasible region where the objective function can be estimated. Finally, the objective function is maximized until reaching the optimal point, represented by the green dot.

The most suitable algorithm to find the global optima depends on the complexity of the objective function. If the objective function is convex, gradient-based approaches are efficient at finding global optima. However, if the objective function is non-convex, stochastic search strategies are more appropriate in order to avoid being trapped in local optima. Non-Linear Programming by Quadratic Lagrangian (NLPQL) is a special implementation of the Sequential Quadratic Programming (SQP) method for constrained

optimization (Schittkowski 1986). At each major iteration, a quadratic approximation of the Lagrangian function and a linearization of the constraints is made. Then, a Quadratic Programming (QP) subproblem is generated whose solution is employed to define a search direction. An overview of SQP can be found in (Fletcher 1987), (Gill, Murray, and Wright 1981), and (Powell 1983). The Lagrangian function $\mathcal{L}(\boldsymbol{\theta}, \lambda)$ employed is expressed in Equation (10).

$$\mathcal{L}(\boldsymbol{\theta}, \boldsymbol{\lambda}) = f(\boldsymbol{\theta}) + \sum_i \lambda_i h_i(\boldsymbol{\theta}) \tag{10}$$

where λ_i are the Lagrangian multipliers, h_i are the inequality constraint functions ($h_i(\boldsymbol{\theta}) < 0$) and i is the number of inequality constraint functions. For each measurement, two inequality constraint functions are defined to ensure that the residual between prediction and measurement falls within upper and lower threshold bounds ($T_{i,low} \leq\ g(x_i, \boldsymbol{\theta}) - y_i \leq\ T_{i,high},\ \forall i = 1, 2, \dots, n_y$). Furthermore, for each parameter, two inequality constraint functions are defined to ensure that parameter values are within prior bounds ($\theta_{j,min} \leq \theta_j \leq\ \theta_{j,max},\ \forall j = 1, 2, \dots, n_p$).

A set of parameter values $\boldsymbol{\theta}^*$ is a local maximum if there exists a unique vector of Lagrangian multipliers $\boldsymbol{\lambda}^*$ such that:

1) $\nabla_{\boldsymbol{\theta}} \mathcal{L}(\boldsymbol{\theta}^*, \boldsymbol{\lambda}^*) = 0$ (11)

2) $\lambda_i^* \geq 0, \quad \forall i$ (12)

3) $\lambda_i^* h_i(\boldsymbol{\theta}^*) = 0, \quad \forall i$ (13)

4) $h_i(\boldsymbol{\theta}^*) \leq 0, \quad \forall i$ (14)

5) The Hessian matrix $\nabla^2_{\boldsymbol{\theta}\boldsymbol{\theta}} \mathcal{L}(\boldsymbol{\theta}^*, \boldsymbol{\lambda}^*)$ is positive definite

where $\nabla_{\boldsymbol{\theta}}$ denote the partial derivative of the following function with respect to $\boldsymbol{\theta}$.

These conditions are referred to as the Karush-Kuhn-Tucker conditions (Kuhn and Tucker 1951). This methodology is repeated with several starting points in order to determine either that the solution has converged to the global maximum or that stochastic search methods are necessary.

Generally, this gradient-based optimization method does not require sampling of the parameter space, compared with traditional implementations of EDMF using LHS that necessitate dense sampling to have a good representation of the candidate-model sub-domain (Proverbio et al 2017). Thus, it is less time

consuming than traditional implementations of error-domain model falsification when few objectives need to be optimized (few limit-state criteria).

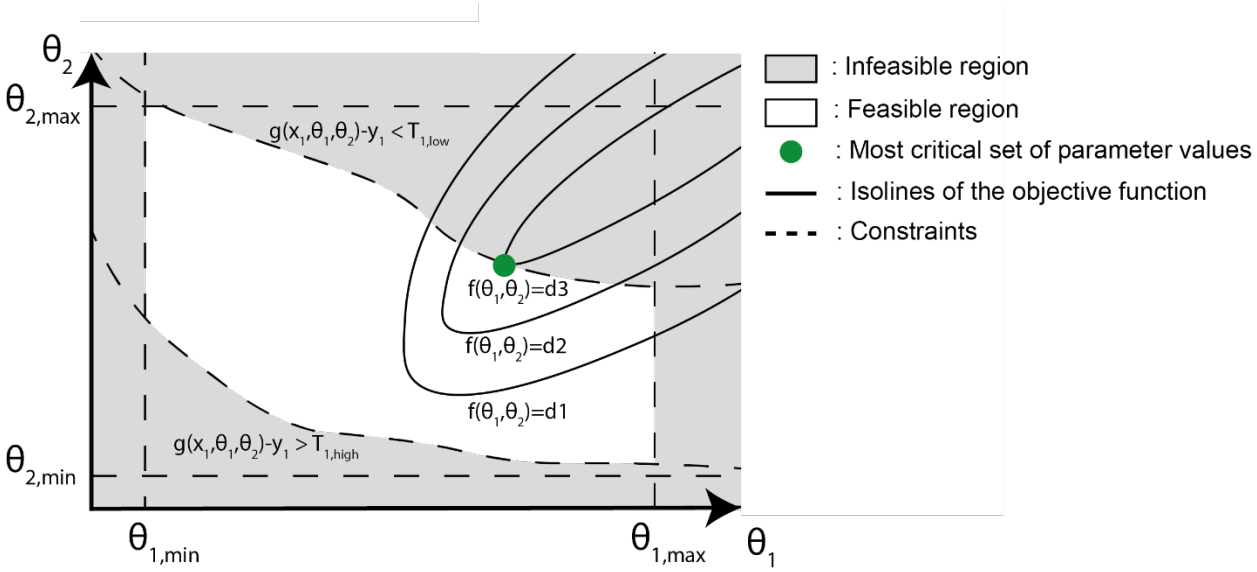

Figure 1: Illustrative example of constrained optimization where $g(x_1, \theta_1, \theta_2)$ is the predicted value of the finite element model at the sensor location x_1 using the load of the trucks and $f(\theta_1, \theta_2)$ is the objective function that needs to be maximized (e.g. stress at the bottom of the most-loaded beam using the load of the Eurocodes). The dark lines are isolines of the objective function.

2.2.1 New framework for ultimate limit state (ULS) verification

Figure 2 presents the new framework for improving the estimation of the load capacity of existing bridges at the ULS using measurements. Two finite element models need to be built for constrained optimization. The first model (FEM1 in Figure 2) describes the behaviour of the bridge under test loads and is used to provide constraints to the parameter domain using the measurement data. This model is used to evaluate the function g when parameter values are varied. This model considers elastic behaviour of materials as the loads of the test have been fixed to avoid cracking.

The second finite element model, FEM2, describes the behaviour of the bridge under the load configuration of the codes and is used to find the most critical set of parameter values for any ultimate limit state. This model is used to evaluate the function f when parameter values are varied. This model also considers elastic behaviour of materials in order to reduce computation time related to the optimization process. If the convergence criterion of the optimization algorithm is not reached, a new generation of parameter-value set

has to be generated using NLPQL (Section 2.2). The parameterization might differ between the two finite-element models (FEM1 and FEM2). For instance, the bearing stiffness might affect significantly the bridge behaviour during the test and, thus, they should be modelled in the first model in order to identify unbiased parameter values. However, for the ultimate limit state verification, free rotation should be used for bearing conditions because the bearing stiffness identified during the test might be due to sticky bearing devices at low load levels.

Finally, a third model (FEM3 in Fig.2) is used for estimating the load capacity of the bridge using a non-linear finite element analysis with the most critical parameter-value set obtained with constrained optimization. This last model is only used once the most critical parameter-value set has been found. In this paper, the most critical set of parameter values at the ULS corresponds to the parameter-value set that provides the highest bending stresses in the most-loaded beam using the second finite element model. A quantitative example is provided in the section that describes the case study. Shear failure is assumed to be not critical in this context. Furthermore, it is assumed that the most critical set of parameter values obtained with an elastic analysis (second finite element model) provides the most critical results for input into a non-linear finite element analysis (third finite element model).

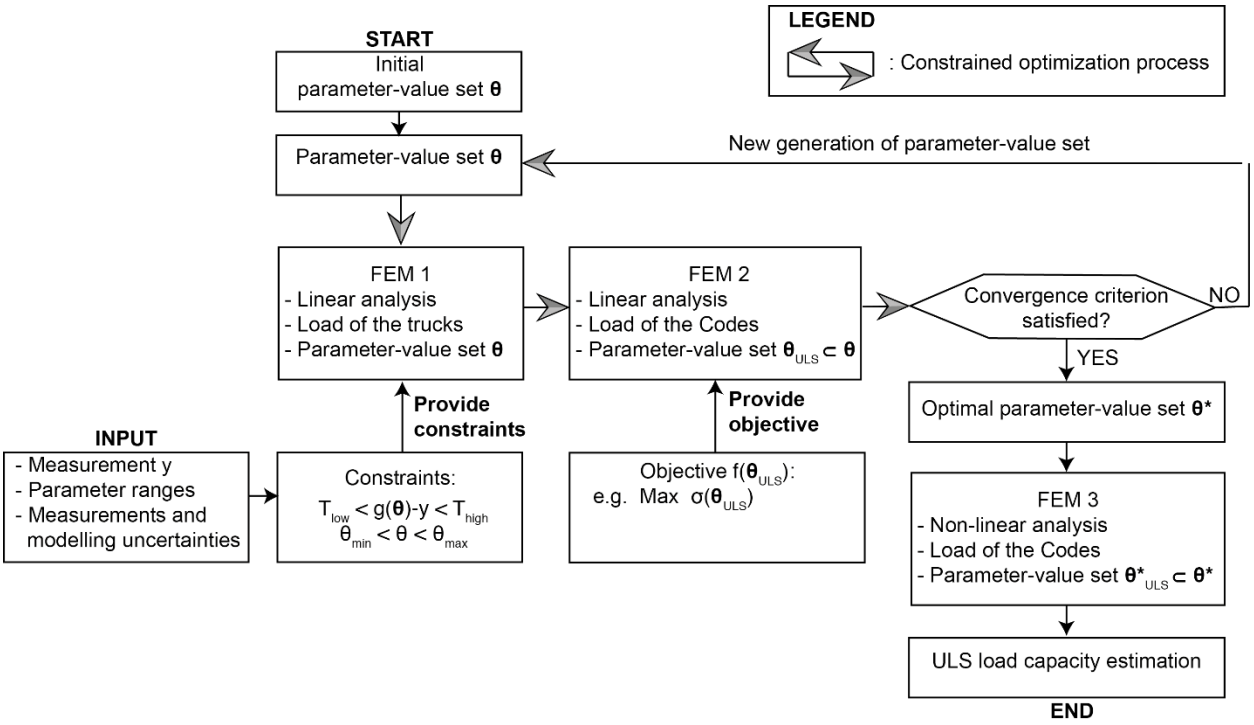

Figure 2: New framework for estimating the bending load capacity of existing reinforced concrete structures at the ultimate limit state. The thresholds of EDMF are used to constrain the parameter-value set θ in FEM1. The parameter-value set θ_{ULS} in FEM2 is a subset of θ and is used for the non-linear analysis in FEM3.

2.2.2 New framework for serviceability limit state (SLS) verification

It is often sufficient to check the serviceability limit state qualitatively using visual inspection and noting the experience of end users if loading remains unchanged (for example, see SIA 269 2011). However, if the live loads are expected to increase, the serviceability limit state should be verified using serviceability requirements of current codes. In Singapore, traffic loads have increased significantly in recent years and will further increase in the future ("Land Transport Authority. Master Plan 2013. Singapore," n.d.). Therefore, verification of serviceability/durability (cracking) requirements is useful and knowledge of reserve capacity may lead to lower costs and improved planning of inspection and maintenance activities.

Figure 3 presents the framework to estimate the load capacity of existing reinforced concrete structures at the serviceability limit state. In this framework only two models are considered. The first model (same model as FEM1 in Figure 2) is used to simulate the behaviour of the bridge under the test loads. The second model (FEM4 in Figure 3) is employed to predict the behaviour of the bridge under the loads defined in the codes for SLS verification.

Both models are defined by elastic material properties and by the same set of parameters. The stiffness of bearing devices and the contribution of non-structural elements such as barriers are considered in both models. In this framework, the objective function depends on the requirements that need to be satisfied at the serviceability limit state. For instance, a requirement is the maximum stress at the bottom of the most-loaded pre-stressed beam in order to avoid cracking of concrete.

This framework is used in Section 3.7 for the assessment of the serviceability limit state.

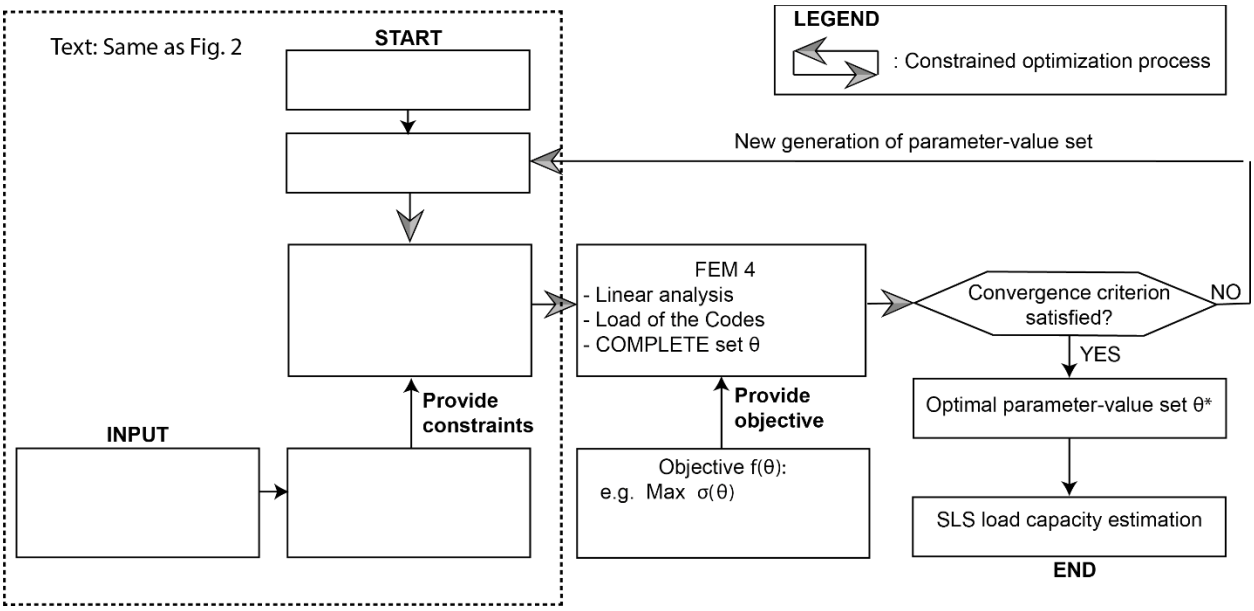

Figure 3: New methodology for estimating the load capacity of existing reinforced concrete structures at the serviceability limit state. With respect to Figure 2, the only difference is in the FEM4 where the complete set of parameters is used in the objective function, compared with only a subset in Figure 2.

3 Case study

3.1 Description

The load capacity of a pre-stressed bridge in Singapore at the ultimate and serviceability limit state is assessed in this paper. This pre-stressed concrete bridge is composed of 4 hollow beams carrying three unidirectional traffic lanes over a simply-supported span of 32 meters. Each beam includes one parabolic post-tensioning tendon in each web and 42 pre-tensioning tendons in the bottom flange.

The principal characteristics of the bridge, the load-test configuration and the sensor configuration are presented in Figure 4.

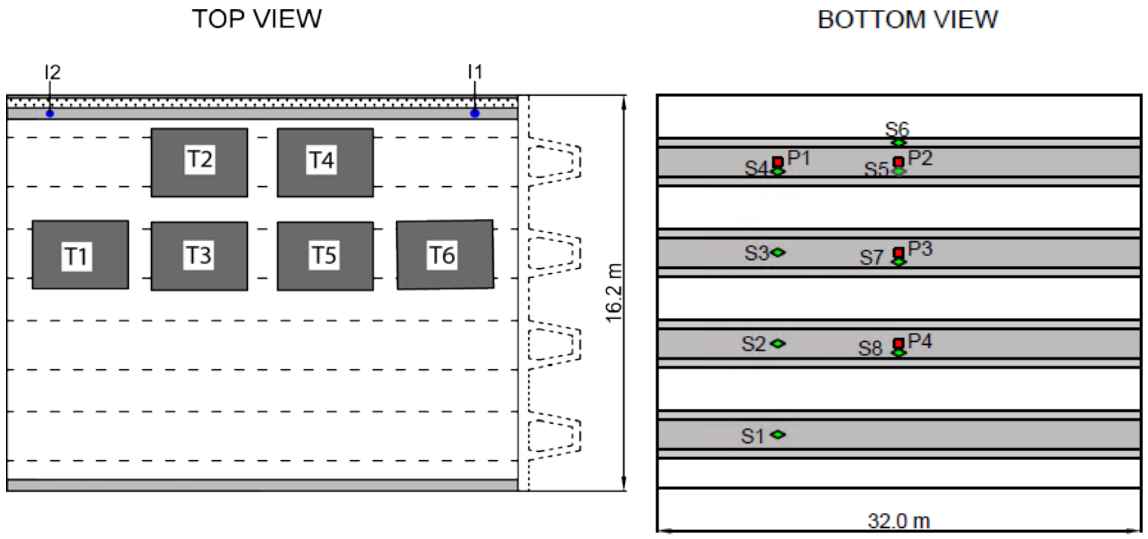

Figure 4: Bridge characteristics as well as load-test and sensor-network configurations, where Ti represents the position of each truck, I_i the inclinometers on one parapet, P_i the deflection targets and S_i the strain gauges distributed on the 4 beams. Each truck is 8m long and there is a uniform space of 1.2m between trucks.

A static load test has been carried out to update a finite element model of the bridge. Figure 5 presents a photograph of the static load test. This static load test involved 6 trucks (Ti) of approximatively 32 tons located on the deck of the bridge. The sensor configuration consisted of 2 inclinometers (I_i) on one parapet, 4 deflection targets (P_i) and 8 strain gauges (S_i) distributed on the 4 beams. A laser tracker was positioned on the road below the bridge and used to measure deflections of the deflection targets. The sensor configuration was chosen based on engineering judgement. These measurements will be used in Section 3.2 for falsification of model instances using EDMF.

Figure 5: Photograph of a static load test performed on a reinforced concrete bridge in Singapore

Figure 6 presents the bridge characteristics as well as the finite element model of the bridge. The bridge has been modelled with ANSYS Workbench using solid elements.

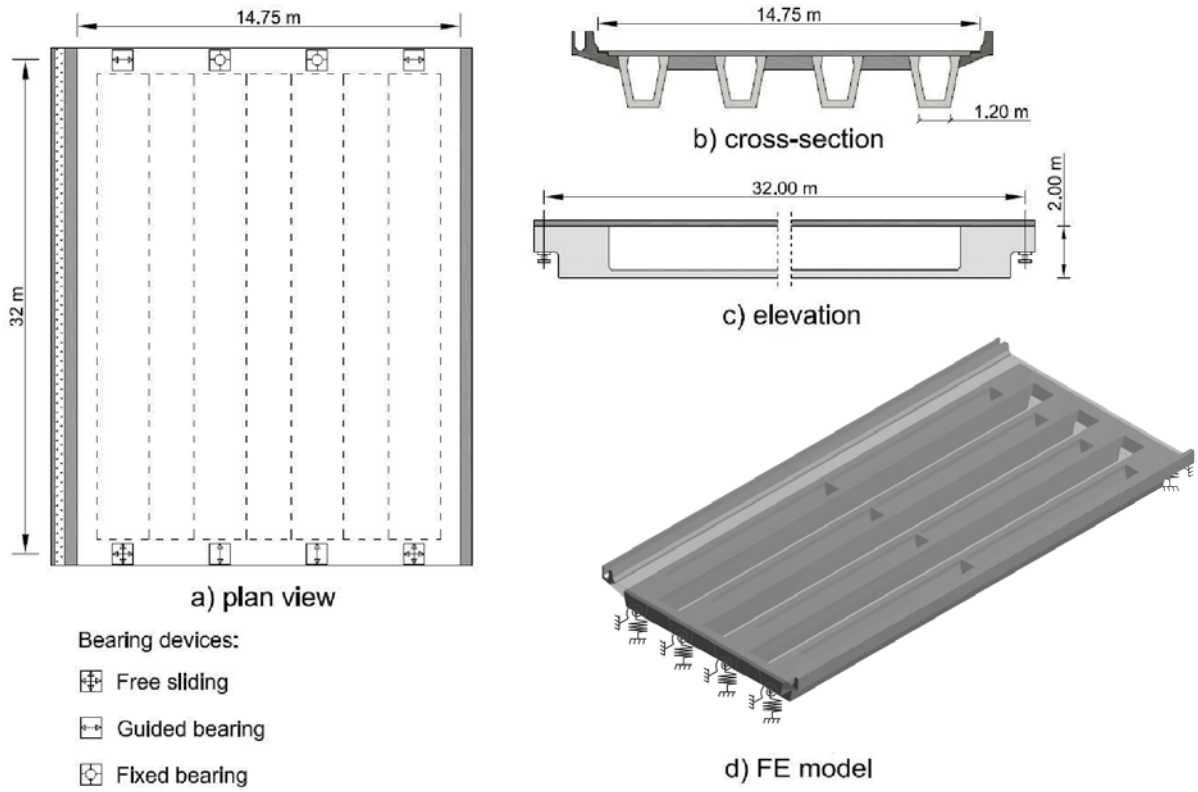

Figure 6: a) Plan view, b) cross-section, c) truncated elevation of a beam and d) finite element model of the bridge

3.2 **Error-domain model falsification**

Measurements have been used to update a finite element model of the bridge using the error-domain model falsification methodology. The initial parameter set was chosen following a sensitivity study. Initially, 8 parameters were chosen for consideration. Following the sensitivity analysis, 5 were retained since each of them demonstrated a relative importance of at least 8 % in relation to the response at sensor locations. These parameters are: 1) the elastic modulus of site-cast concrete of the deck and diaphragms E_{poured}, 2) the elastic modulus of the precast concrete of the beams $E_{precast}$, 3) the elastic modulus of the concrete of the barrier $E_{barrier}$, 4) the rotational stiffness of the bearing devices $Rot.Stiff.$ and 5) the vertical stiffness of the bearing devices $Vert.Stiff.$ Values of bearing stiffness are sampled in the logarithmic scales in order to avoid selecting mostly high values of bearing stiffness. The initial intervals of the parameters have been estimated using conservative engineering judgment and are presented in Table 1.

In this 5-parameter space, 2000 initial model instances were generated using the Latin Hypercube Sampling (LHS) method.

Table 1: Lower and upper bounds for parameter values

	$E_{barrier}$ [MPa]	**E_{poured} [MPa]**	**Rot. Stiff. [log(Nmm/rad)]**	**Vert. Stiff. [log(N/mm)]**	**$E_{precast}$ [MPa]**
Lower bound	3000	20000	9	8	25000
Upper bound	40000	35000	13	11	50000

For the identification of parameter values, non-structural elements such as barriers and the stiffness of bearing devices are considered in order to avoid biased identification of parameter values. In this particular case study, the barriers are the only relevant non-structural elements that affect structural behaviour. For example, the pavement elastic modulus does not affect significantly the bridge behaviour and are not considered here. The parameter ranges for the young modulus have been chosen large enough to ensure that the worst-case scenario will be covered. The rationale for the bounds of barrier stiffness is that the barriers have a connection that is in between sliding and perfectly fixed with the deck. For the bearing rotational stiffness, the maximum value corresponds to a constrained support and the lowest value corresponds to a pinned support. Indeed, in structures that are decades old, the support conditions no longer behave as pin-rollers (Huseynov et al. 2017). The same logic is applied to the vertical stiffness.

Upper and lower bounds of model-class uncertainties and measurement uncertainties are presented in Table 2. Uniform distributions are assumed between those bounds. Bounds are defined either as an absolute value or a percentage of the measured value. Modelling uncertainties have been estimated based on engineering judgment and literature review using conservative assumptions. As strain gauges measure local behavior, a source of uncertainty associated with local variability has been added for these sensors. Deflection targets and inclinometers are not concerned by this additional uncertainty since they do not measure a local behavior. Sensor accuracy is taken from sensor specifications and sensor repeatability is estimated through making several measurements under the same load configuration. For strain gauges and inclinometers, uncertainties originating from their installation have been estimated using engineering judgment and from field observations (e.g. strain gauges unaligned with beam orientation). Deflection measurements do not involve additional installation uncertainty since the laser tracker records the relative displacement of targets, which is not affected by installation procedures.

Table 2: Modelling and measurement uncertainties

			Deflection targets	**Strain gauges**	**Inclinometers**
Modelling uncertainties	Model simplifications and FEA	Min	-5 %	-5 %	-5 %
		Max	13 %	13 %	13 %
	Mesh refinement	Min	-1 %	-1 %	-1 %
		Max	1 %	1 %	1 %
	Local variability	Min	-	-5 %	-
		Max	-	5 %	-
	Additional uncertainty	Min	-1 %	-1 %	-1 %
		Max	1 %	1 %	1 %
Measurement uncertainties	Sensor accuracy	Min	-0.1 mm	-6 μrad	-5 μrad
		Max	0.1 mm		
	Sensor repeatability	Min	-0.123 mm	6 μrad	5 μrad
		Max	0.123 mm		
	Sensor installation	Min	-	0 %	-5 %
		Max	-	11 %	5 %

Figure 7 presents a parallel-axis plot in which parameter values and predictions are plotted. Measurements obtained during the test, threshold bounds computed with Equation (5) and prediction bounds computed with Equation (6) are also presented in this figure. Over the 2000 initial model instances generated by Latin Hypercube Sampling, only 9 model instances satisfy the condition stated in Equation (4). They are retained as candidate models. The vertical stiffness and the elastic modulus of precast concrete are well identified. Values of vertical stiffness have been reduced from [8 log(N/mm); 11 log(N/mm)] to [8.39 log(N/mm);

8.55 log(N/mm)]. For the elastic modulus of the precast concrete, values have been reduced from [25 GPa; 50 GPa] to [39 GPa; 50 GPa]. However, the range of parameter values for the elastic modulus of the poured concrete has not been reduced after falsification.

Sensor P4 is used to test the EDMF methodology through a cross validation. P4 data were not used to infer the candidate model set but only to test whether its measurement falls within prediction bounds, estimated according to Equation (6). As shown in Figure 7, the measured value at test sensor P4 falls inside the prediction interval, consolidating the prior assumption made on modelling-uncertainty magnitudes.

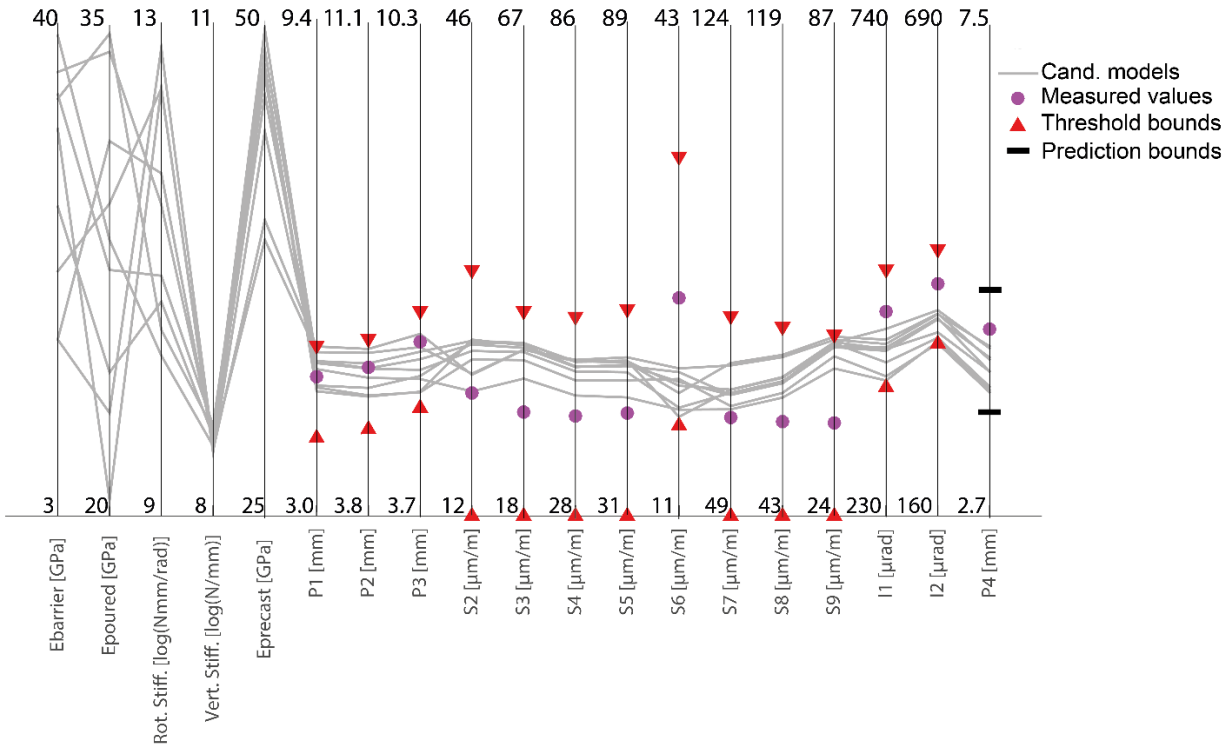

Figure 7: Parallel axis plot presenting the results of EDMF

3.3 Implementation of the new methodology for ultimate limit state verification

In this section, the results of the new framework are presented and compared with those obtained with the traditional implementation of EDMF (Section 3.2).

The finite element model of the bridge described in the previous section (Figure 6(d)) is used to simulate the behaviour of the bridge under the test loads (referred to as FEM1 in Figure 2). The initial parameter-value set is constituted by 5 parameters. Their respective ranges have been detailed in the previous section.

A second finite element model, referred to as FEM2 in Figure 2, has been made to simulate the bridge behaviour under the loads of the code and is used to evaluate the objective function. As the bending loading capacity is studied in this paper, the variable predicted by FEM2 that needs to be maximized is the stress at the bottom of the most loaded beam. In this second finite element model, design assumptions have been used for boundary conditions because the bearing stiffness identified during the test might be due to sticky bearing devices at low load levels. As little information regarding the structural strength of the joints between barrier blocks were available, barriers were not considered in this model. Thus, among the five parameters used during identification, only two parameters affect predictions of the second model. Those two parameters are the elastic modulus of the precast concrete and the elastic modulus of the poured concrete, which affect the lateral distribution of loads as well as the neutral axis of the section. The objective is to find the set of parameter values that maximizes the bending stress predicted by the second finite element model at the bottom of the most-loaded beam given constraints from measurements (see Figure 2). It is assumed that the most critical set of parameter values obtained with an elastic analysis (FEM 2) provides the most critical results in a non-linear finite element analysis (FEM 3).

As explained previously, NLPQL has been used for constrained optimization in order to find the most critical set of parameter values given measurement constraints. The NLPQL algorithm needs to be repeated with several starting points in order to ensure that the optimal model is not a local optimum of the objective function (e.g. maximizing bending stress in the most-loaded beam). In this case study, NLPQL has been run with 10 starting points. All converged to the same set of parameter values.

In NLPQL, the gradient of the objective function in each parameter dimension is computed at each iteration using the forward finite difference approximation. Then, a simulation sample is generated in the direction that increases the objective function. As five parameters are considered in this study, six simulations are executed by iteration for each finite element model (first and second model) and, thus, a total of twelve simulations are executed by iteration.

Figure 8 presents the stress at the bottom of the most-loaded beam predicted by FEM2 (objective function to maximize) with respect to the number of iterations of the constrained optimization algorithm for one starting point. This figure also presents the deflection predicted by FEM1 at P1 during the constrained optimization process as well as the constraints provided by measurements. When the starting values of parameters are assigned to the model, the predicted deflection P1 falls outside the threshold bounds. At convergence of the algorithm, the constraint is satisfied and the objective function has been maximized.

Only the dead load and the traffic load are considered in FEM2, without considering the effects of the pre- and post-tensioning tendons. Thus, high tensile stress is predicted at the bottom of the most-loaded beam in the elastic analysis. In non-linear analysis (FEM3), the effect of post-tensioning will be considered to estimate the load capacity.

The upper threshold bound for deflection at P1 is the most restrictive (also referred to as active constraint). For each starting point, 5 to 9 iterations are needed to reach convergence. Thus, a total of 60 to 108 simulations are needed for each starting point, which require around 3 to 5 hours of simulations using 12 processors. Using 10 starting points, a total number of 750 evaluations have been executed. This number is approximately one third of the 2000 evaluations needed for the traditional implementation of EDMF where LHS is used to generate model instances (Section 3.2).

Results obtained with non-linear FEM, using the most critical set of parameter values obtained with constrained optimization, are presented in Section 3.6.

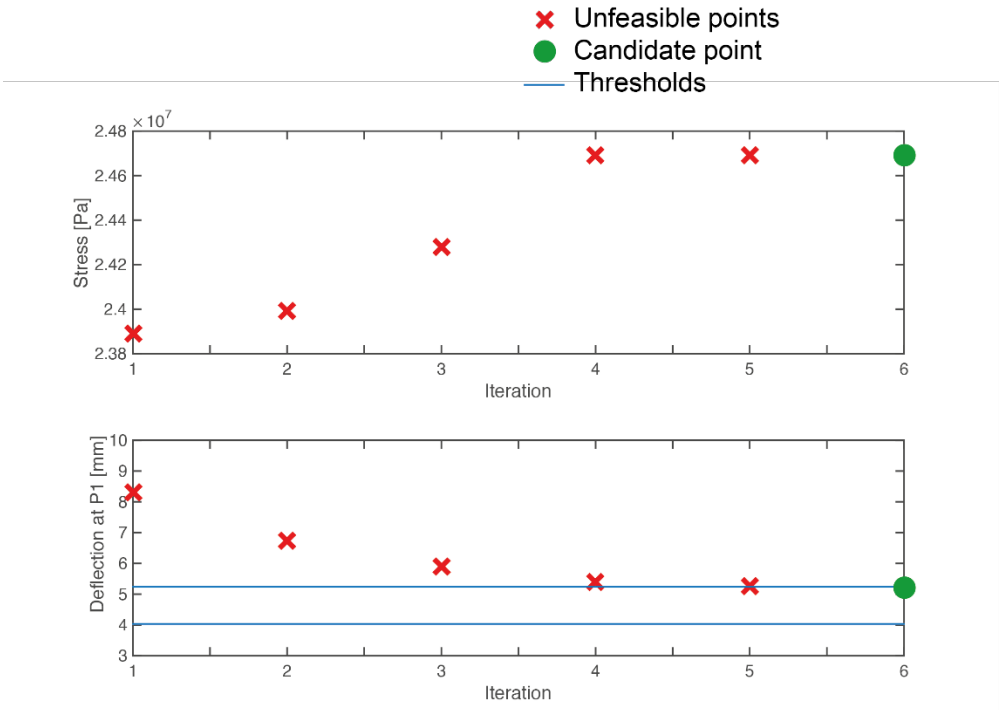

Figure 8: Stress at the bottom of the most-loaded beam predicted by the second model (objective function) with respect to the number of iterations of NLPQL (top) and deflection predictions at P1 (active constraint) with respect to the number of iterations of NLPQL (bottom)

Figure 9 presents a parallel-axis plot where parameter values and predictions are plotted for the candidate models of EDMF (grey lines) and for the model obtained with the new methodology (dashed line). This line corresponds to the results obtained with the last set of parameter values evaluated before reaching convergence (green dot in Figure 8). As presented in Figure 8, the constraint associated with the predicted deflection at P1 is the most restrictive (active constraint).

The parameter-value set obtained with constrained optimization and assigned to the second finite element model predicts higher stress at the bottom of the most-loaded beam than those obtained with the candidate models of EDMF while providing predictions that are within threshold bounds. This set provides a value of elastic modulus for the poured concrete corresponding to the lower bound of its initial interval and a value of elastic modulus for the precast concrete corresponding to the upper bound of its initial interval.

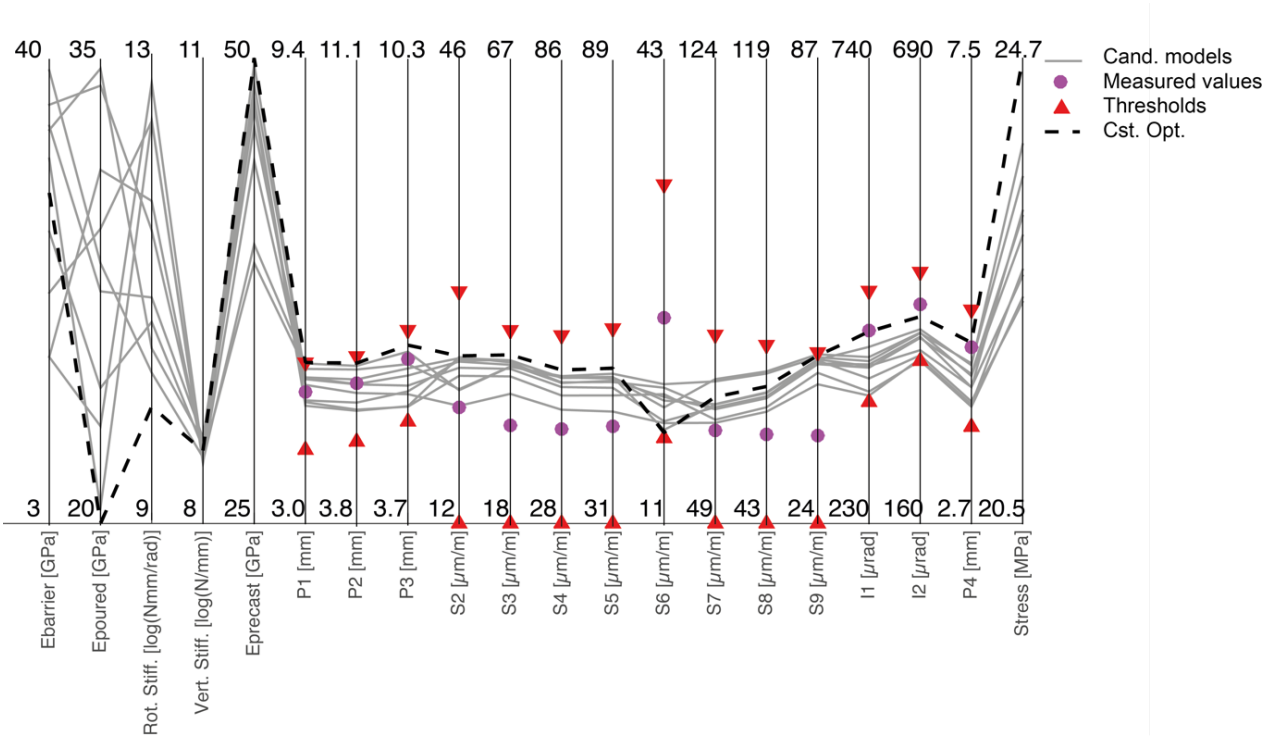

Figure 9: Parallel axis plot presenting the results of EDMF and the new methodology (Cst. Opt.)

3.4 Sensitivity of results to prior definition of uncertainties

The choice of modelling uncertainties is based on engineering judgment. In this section, the impact of uncertainty ranges on the set of parameter values obtained using constrained optimization and, ultimately, on the final assessment of the loading capacity (Section 3.6) is assessed.

In Figure 10, uncertainties have been reduced in order to assess the sensitivity of results to uncertainty misevaluation. Uncertainties associated with FEM simplification have been reduced from [-5%, +13%] to [-3%, +5%]. This choice can be justified because 1) the finite element model incorporates secondary elements, such as barriers and diaphragms, 2) the most important parameters, including boundary conditions, are parameterized and 3) solid elements are used. Furthermore, the parameter range for the elastic modulus of barrier has been reduced from [0 GPa, 40 GPa] to [0 GPa, 25 GPa]. This choice can be justified because 10-mm joints made of bitumen sealant are placed between barrier blocks, which reduce their stiffness. However, more tests and analyses would be needed to confirm these hypotheses.

The parameter-value set obtained with the new methodology using the first definition of uncertainties does not provide predictions within the new threshold bounds at locations P1, P2 and S6. Using the second definition of uncertainty, the lower bound of poured-concrete stiffness has been increased and the upper bound of the precast-concrete stiffness has been decreased resulting in lower stress at the bottom of the most-loaded beam predicted using the second model (axis on the right in Figure 10). The stress in the most-loaded beam predicted with the most critical model obtained using the new estimation of uncertainty is 5.8% lower than the stress predicted by the most critical model obtained using the original estimation of uncertainty. The impact on the prediction of load capacity using NLFEA is presented in Section 3.6.

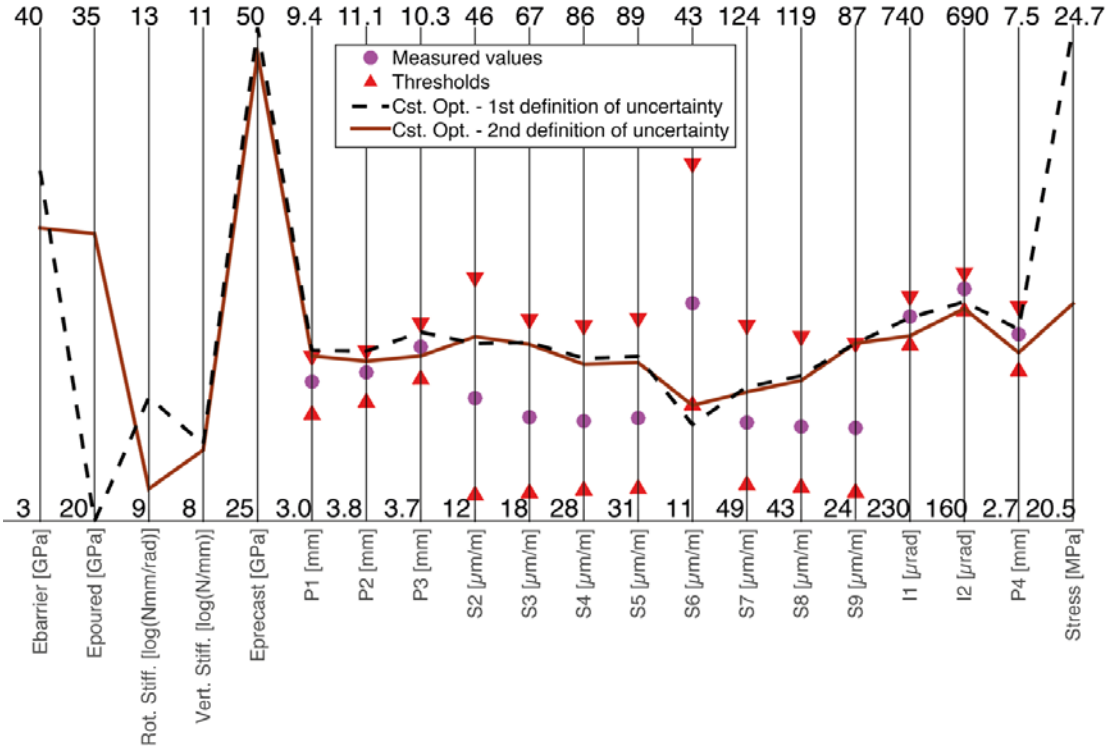

Figure 10: Parallel axis plot presenting the results of the new methodology using the original and the new definition of modelling uncertainty

3.5 Comparison with residual minimization

In this section, previous results are compared with those of residual minimization using NLPQL (Schittkowski 1986). In residual minimization, the goal is to minimize the normalized root mean square error (NRMSE) between predictions and measurements. Equation (15) presents the objective function to be minimized.

$$\boldsymbol{\theta}^* = \min_{\boldsymbol{\theta}} \frac{1}{n_y} \sqrt{\sum_{1}^{n_y} \left(\frac{g(x_i, \boldsymbol{\theta}) - y_i}{g(x_i, \boldsymbol{\theta})}\right)^2} \tag{15}$$

NLPQL has been performed with 10 starting points. Seven of them provide the same value of NRMSE (=0.08) while the three others provide higher values of NRMSE. This difference can be due to local minima or convergence issues. Figure 11 presents the convergence graph for only 5 of those points for clarity. On average, 22 iterations (132 simulations) are needed to reach convergence. In residual minimization, no weight has been used and, thus, it is assumed that the information content of each observation is the same

and that the information content of one observation is independent of all others. On the contrary, in approaches based on EDMF such as the one proposed in this paper, the information content of each observation is reflected in the width of the threshold bounds. Furthermore, approaches based on EDMF are robust to misevaluation of error correlation between sensor locations (Goulet and Smith 2013).

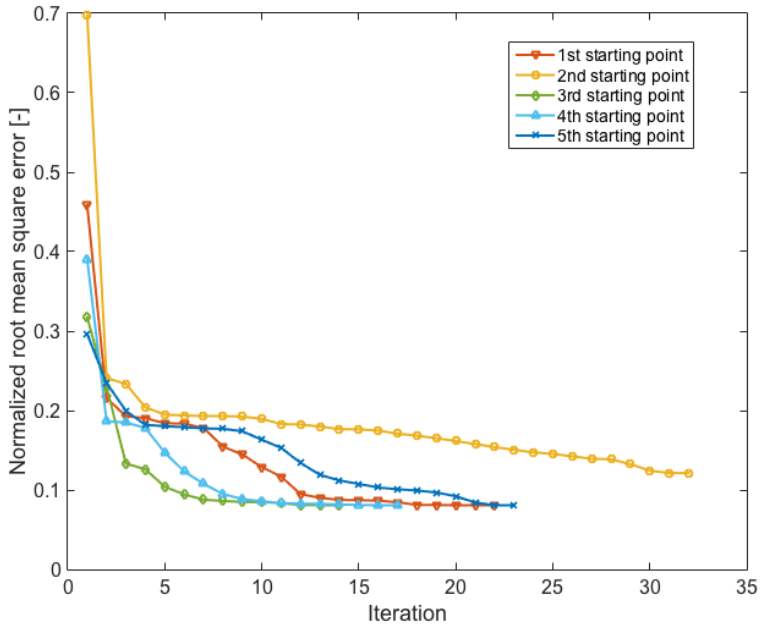

Figure 11: Normalized root mean square error with respect to the number of iterations of NLPQL

Figure 12 presents a parallel-axis plot in which parameter values and predictions are plotted for the candidate models of EDMF (using the original definition of uncertainty) and for the model obtained with residual minimization. The “optimal” model obtained with residual minimization predicts a lower value of stress at the bottom of the most-loaded beam under the loads of the code than those identified with EDMF and with the new methodology. Furthermore, this model does not provide predictions that fall within threshold bounds for the two inclinometers. As opposed to residual minimization, EDMF and constrained optimization leads to a set of parameter values that provides predictions within uncertainty bounds for each measurement data, giving confidence on the parameter values identified and subsequent predictions. The impact of the model-updating methodology on the reserve capacity is presented in Section 3.6 for ULS verification and in Section 3.7 for SLS verification.

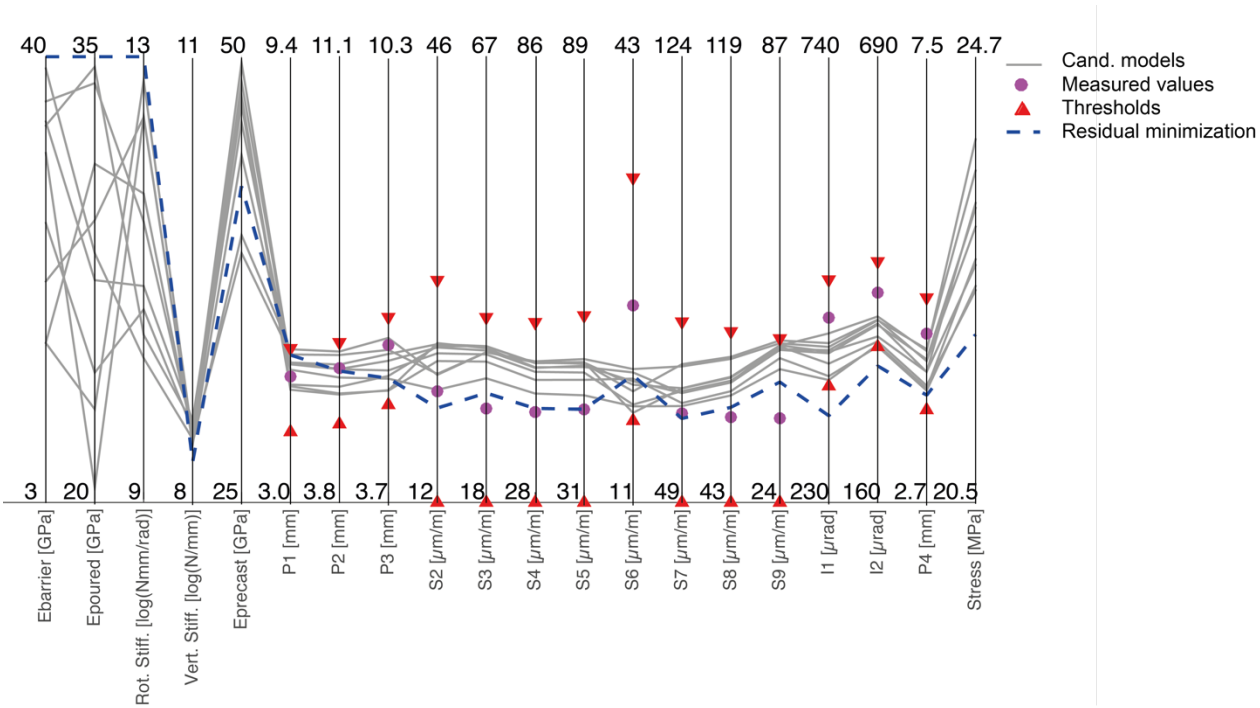

Figure 12: Parallel axis plot presenting the optimal model obtained with residual minimization and the candidate models obtained with EDMF.

3.6 Load capacity estimation using non-linear finite element analysis

In this section, non-linear finite element analyses (referred to as FEM3 in Figure 2) are performed in order to assess the bending load capacity of the bridge at the ultimate limit state using the parameter values obtained with constrained optimization and residual minimization.

Figure 13 presents the model used to assess the load capacity at the ultimate limit state. In this model, the barriers are not considered explicitly and the bearings are modelled as pinned supports. Instead, the weight of the barriers is modelled by applying a load on the bridge at the location of the barriers. The parabolic post-tensioning tendons and the linear pre-tensioning tendons have been explicitly modelled in the simulation. Pre-tensioning and post-tensioning tendons have been modelled using beam elements. Then, the nodes of the beam elements are merged to the nodes of the solid concrete elements. The nodes of both elements have to be close enough (lower than a defined tolerance) in order to be merged. This is done by slicing the solid geometry in sub-parts in order to create edges that are coincident with the beam elements. Then, the same number of subdivisions are imposed for the beam elements and the edges of the solid bodies in order to have coincident nodes. Finally, the coincident nodes are merged. The reinforcement bars have not been modelled. Thus, the load capacity estimated in this paper is a lower bound estimate.

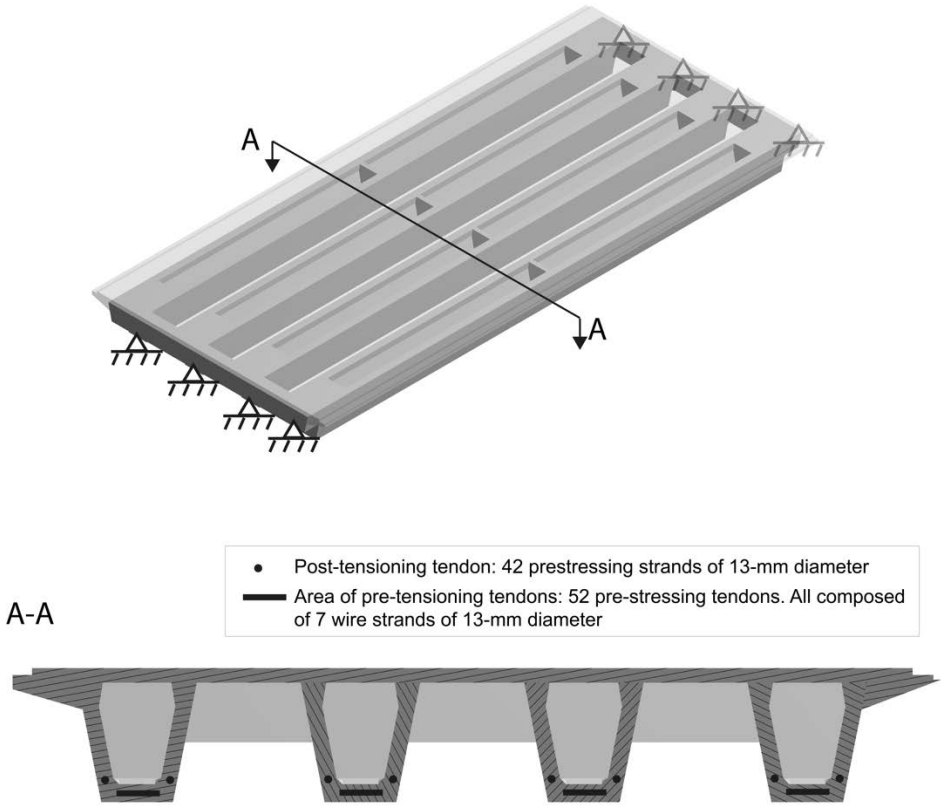

Figure 13: Finite element model used to assess the load capacity at the ultimate limit state

The Eurocodes with the Singaporean National Annexes (SS EN 1991-2 Eurocode 1 2012; SS EN 1992-2 Eurocode 2 2012) are currently used in Singapore for the design of new bridges. The loads mentioned in these documents were used to estimate load capacity.

In this model (FEM3), strength properties are defined using codes. Structural properties of steel tendons are modelled using elastic perfectly plastic constitutive laws and the structural properties of concrete are modelled using a Drucker-Prager plasticity model that is defined by three parameters: 1) the uniaxial compressive strength f_{cd}, 2) the uniaxial tensile strength f_{ctd} and 3) the biaxial compressive strength f_{c2cd}. Design strength of concrete and tensioning tendons are reported in Table 3. Furthermore, the partial-safety-factor method has been used for verification. Limitations regarding the use of the partial-safety-factor method with non-linear finite element analyses are mentioned in Section 4.

Table 3: Design strength of concrete and post- and pre-tensioning tendons

	f_{cd} [MPa]	f_{ctd} [MPa]	f_{c2cd} [MPa]		f_{pd} [MPa]
Poured concrete	27	1.7	31	Pre-tensioning tendons	1374
Precast concrete	16.7	1.2	20	Post-tensioning tendons	1273

The load factor is employed to assess the reserve capacity of the bridge and corresponds to the extra-carrying capacity of the bridge for bending verification at the ultimate limit state. The load factor LF is defined in Equation (16).

$$LF = \frac{Q_{failure}}{Q_d} \tag{16}$$

Where Q_d is the design traffic load (with partial safety factors) of the Eurocodes and $Q_{failure}$ is the load at failure obtained with non-linear finite element analysis.

Figure 14 presents the load-displacement curves simulated using FEM3 when parameter values obtained by constrained optimization (Figure 14a and Figure 14b) and residual minimization (Figure 14c) are assigned to the model. Failure is reached when the ANSYS solver diverges. At failure, the pre- and post-tensioning tendons are yielded. Yielding of the post-tensioning tendons occurs before yielding of the pre-tensioning tendons. Concrete crushing (total strain of 3.5‰ in the concrete) does not occur at divergence. However, the strain in the deck has an asymptotic behaviour at divergence and therefore, crushing would have occurred for a similar load factor.

The load factor obtained using constrained optimization with initial and modified uncertainty magnitudes is 1.48 and 1.53 respectively while the load factor obtained with residual minimization is 1.56. This small variation originates from the difference in the identified values of the elastic modulus of poured and precast concrete, which affect the lateral load distribution in the non-linear finite element analysis. These results indicate as expected that the parameters identified using EDMF do not significantly affect the ultimate load capacity.

a) Constrained optimization with initial uncertainty magnitudes

b) Constrained optimization with modified uncertainty magnitudes

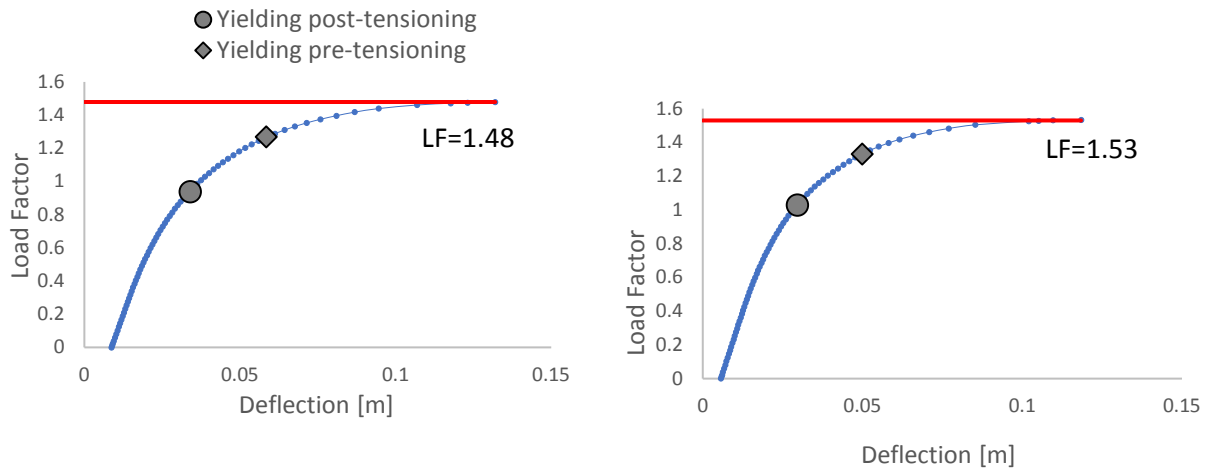

c) Residual minimization

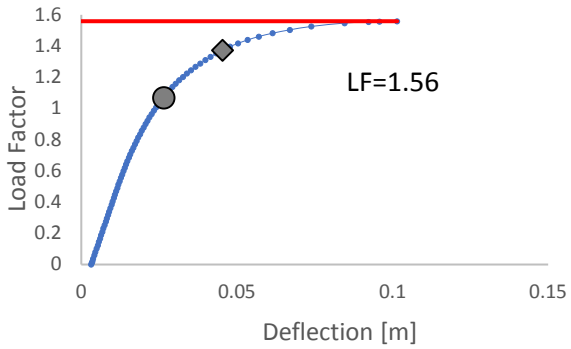

Figure 14: Load factor with respect to the deflection of the most-loaded beam using the set of parameter values provided by each model-updating approach: a) constrained optimization with initial uncertainty magnitudes; b) constrained optimization with modified uncertainty magnitudes; and c) residual minimization

3.7 Implementation of the new methodology for serviceability limit state verification

The methodology described in Section 2.2.2 and Figure 3 is used to estimate the load factor for reserve capacity at the serviceability limit state. Crack control was found to be the critical requirement for this case study. As it is a pre-stressed bridge and considering the exposure class of the bridge, the control of crack width is satisfied by ensuring that no tensile stress occurs in the concrete around bonded tendons.

Figure 15 presents the stress at the bottom of the most-loaded beam with respect to the load factor. The load factor is computed using Equation 16, in which Q_d corresponds to the design traffic load of the Eurocodes at the serviceability limit state. Tensile stress (cracking near prestressing cables) occurs for a load factor of 1.25 for the constrained optimization with the 1st definition of uncertainty magnitude, 1.30 for constrained optimization with the 2nd definition of uncertainty magnitude and 1.55 for residual minimization. The parameter values identified by each model-updating methodology are depicted in Table 4.

Using residual minimization for model updating can significantly affect calculations of load capacity of the bridge at the serviceability limit state, which might lead to unrealistic assessment of cracking vulnerability in existing bridges. Moreover, reduction in modelling-uncertainty magnitudes, which are needed to define constraints in the proposed methodology, leads to an increase of the load-capacity estimate of 5%. Furthermore, for each model-updating methodology, the load factor for the serviceability limit state is consistently lower than the load factor obtained for the ultimate limit state. This indicates that serviceability is the critical limit state for this case.

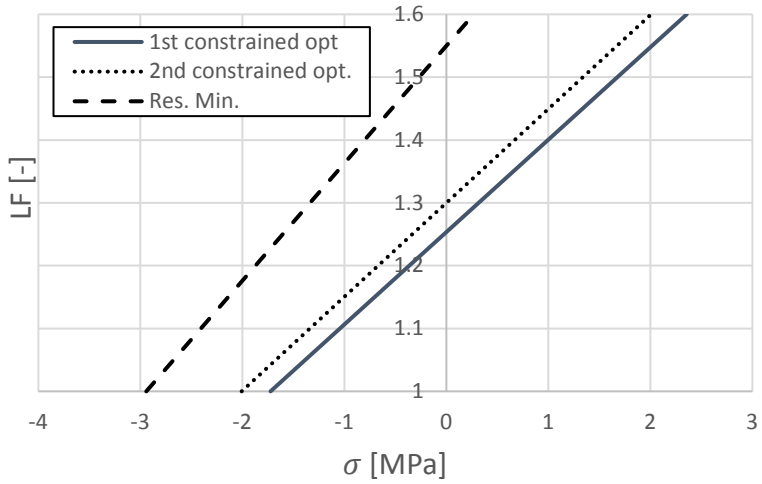

Figure 15: Stress at the bottom of the most-loaded beam with respect to the load factor

	$E_{barrier}$ [MPa]	E_{poured} [MPa]	Rot. Stiff. [log(Nmm/rad)]	Vert. Stiff. [log(N/mm)]	$E_{precast}$ [MPa]
Constrained optimization – 1st definition of uncertainty magnitudes	26139	20000	9	8.49	49929
Constrained optimization – 2nd definition of uncertainty magnitudes	35979	20379	9.55	8.49	49152
Residual minimization	40000	35000	13	8.27	42742

Table 4: Parameter values identified using constrained optimization and residual minimization

4 Conclusions and future research

Sensing has the potential to improve sustainability through quantification of previously unknown reserve capacity. In this paper, a new methodology has been proposed to update models of structural systems using measurements. Measurements taken during a static load test have been used to update a finite element model. This methodology, which is based on EDMF and constrained optimization, has been used to provide robust assessment of the load capacity of a reinforced concrete bridge at the ultimate and serviceability limit state. This methodology is expected to be useful for other complex critical infrastructure systems.

As opposed to residual minimization, constrained optimization leads to a set of parameter values that provides predictions within uncertainty bounds for each measurement data, giving confidence on the parameter values identified and subsequent predictions. The set of parameter values obtained with constrained optimization also provides a lower load capacity than traditional implementation of EDMF and residual minimization while satisfying constraints imposed by measurements. It has been shown that residual minimization may over-estimate load capacity of existing bridges if model biases are not considered, especially at the serviceability limit state. At the serviceability limit state, the difference between the load capacity estimated using residual minimization and the one estimated using constrained optimization is up to 30% due to variation in the identified values of parameters. Thus, using residual minimization for model updating can significantly affect calculations of the load capacity of the bridge at the serviceability limit state, which might lead to a dangerous under-estimation of cracking vulnerability in existing bridges.

At the ultimate limit state, the parameters identified using EDMF do not significantly affect the ultimate load capacity. Indeed, load capacity is not significantly affected by element stiffness at the ultimate limit state as compared to the elastic domain (Eamon and Nowak 2002). An important shortcoming is that results from linear-range tests provide limited information for the non-linear ultimate behaviour. Furthermore, there are more unobservable parameters than stated. For example, compressive and tensile strengths of concrete govern the ultimate behaviour; however, value for these parameters are not updated in the proposed framework. Finally, contributions of non-structural elements, such as barriers, and bearing stiffness have not been considered for ultimate limit state verification. However, these elements might contribute significantly the bridge load capacity, from 1.1 to 2.2 times according to (Eamon and Nowak 2002).

The weaknesses of the proposed method can be addressed with additional research. In this paper, the partial-safety-factor method has been used for ultimate-limit-state verification. Two limitations arise when this method is employed in combination with non-linear finite element analysis (Schlune, Plos, and Gylltoft 2012). Firstly, the use of reduced material strength can lead to unrealistic load distribution and failure modes. Secondly, the partial safety factors defined in codes are calibrated for design analysis of beam and column sections and might not reflect well uncertainties involved in non-linear finite element analysis. While the global-safety-factor method partially overcomes these limitations, the coefficient of variation of modelling uncertainties, which is needed to compute the global safety factor, is still not formally defined (Schlune, Plos, and Gylltoft 2012).

Finally, the load capacity estimated with the proposed framework depends on the level of modelling uncertainties at sensor locations. Additional work might improve the evaluation of modelling uncertainties and the choice of initial parameter ranges. Inspection and non-destructive tests should be used to have a better estimation of initial parameter ranges and, thus, improve the estimation of load capacity.

5 Acknowledgements

The research was conducted at the Future Cities Laboratory at the Singapore-ETH Centre, which was established collaboratively between ETH Zurich and Singapore's National Research Foundation (FI 370074016) under its Campus for Research Excellence and Technological Enterprise programme. The authors gratefully acknowledge the support of the Land Transport Authority (LTA) of Singapore for support during load tests.

6 References

1. Atamturktur S, Liu Z, Cogan S, Juang H (2015) Calibration of imprecise and inaccurate numerical models considering fidelity and robustness: a multi-objective optimization-based approach. Struct Multidiscip Optim 51(3):659–671
2. Beck JL, Au SK (2002) Bayesian updating of structural models and reliability using markov chain monte carlo simulation. J Eng Mech 128(4):380–391
3. Beck JL, Katafygiotis LS (1998) Updating models and their uncertainties. i: Bayesian statistical framework. Journal of Engineering Mechanics 124(4):455–461
4. Beven K (2002) Towards a coherent philosophy for modelling the environment. In: Proceedings of the royal society of London. Series A: mathematical, physical and engineering sciences, vol 458. The Royal Society. pp 2465–2484
5. Beven K (2006) A manifesto for the Equifinality thesis. J Hydrol 320(1):18–36
6. Brühwiler E, Vogel T, Lang T, Lüchinger P (2012) Swiss standards for existing structures. Struct Eng Int 22(2):275–280
7. Catbas¸ NF, Kijewski-Correa T, Aktan EA (2013) Structural identification of constructed systems. American Society of Civil Engineers, Reston
8. Cervenka V (2013) Reliability-based non-linear analysis according to Fib model code 2010. Structural Concrete 14(1):19–28
9. Draper D (1995) Assessment and propagation of model uncertainty. J R Stat Soc. 56:45–97
10. Eamon CD, Nowak AS (2002) Effects of edge-stiffening elements and diaphragms on bridge resistance and load distribution. J Bridge Eng 7(5):258–266
11. Fletcher R (1987) Practical methods of optimization. Wiley, New York
12. Gill PE, Murray W, Wright MH (1981) Practical optimization. Academic Press, London, New York
13. Goulet JA, Kripakaran P, Smith IFC (2010) Multimodel Structural Performance Monitoring. J Struct Eng 136(10):1309–1318
14. Goulet JA, Smith IFC (2013) Structural identification with systematic errors and unknown uncertainty dependencies. Comput Struct 128:251–258
15. Huang S-Y, Teghem J (2012) Stochastic versus fuzzy approaches to multiobjective mathematical programming under uncertainty, vol 6. Springer, Berlin
16. Huseynov F, Brownjohn JMW, O'Brien EJ, Hester D (2017) Analysis of load test on composite I-girder bridge. J Civil Struct Health Monit 7(2):163–173
17. Kuhn HW, Tucker AW (1951) Nonlinear programming. In: Proceedings of 2nd Berkeley symposium. Berkeley: University of California Press. pp 481–492
18. Land Transport Authority (2013) Master plan. Land Transport Authority, Singapore
19. Mottershead JE, Link M, Friswell MI (2011) The sensitivity method in finite element model updating: a tutorial. Mech Syst Signal Process 25(7):2275–2296
20. Neves AC, Gonzalez I, Leander J, Karoumi R (2017) Structural health monitoring of bridges: a model-free ANN-based approach to damage detection. J Civil Struct Health Monit 7(5):689–702
21. Nishio M, Marin J, Fujino Y (2012) Uncertainty quantification of the finite element model of existing bridges for dynamic analysis. J Civil Struct Health Monit 2(3–4):163–173
22. Pasquier R, D'Angelo L, Goulet J-A, Acevedo C, Nussbaumer A, Smith IFC (2016) Measurement, data interpretation, and uncertainty propagation for fatigue assessments of structures. J Bridge Eng. https://doi.org/10.1061/(ASCE)BE.1943-5592.0000861
23. Pasquier R, Smith Ian FC (2015) Robust system identification and model predictions in the presence of systematic uncertainty. Adv Eng Inform 29(4):1096–1109
24. Pasquier R, Smith IF (2016) Iterative structural identification framework for evaluation of existing structures. Eng Struct 106:179–194

25. Pimentel M, Brühwiler E, Figueiras J (2014) Safety examination of existing concrete structures using the global resistance safety factor concept. Eng Struct 70:130–143
26. Powell MJ (1983) Variable metric methods for constrained optimization. Mathematical programming the state of the art. Springer, Berlin, pp 288–311
27. Proverbio M, Costa A, Smith FC (2017) Adaptive sampling methodology for structural identification using radial-basis functions. J Comput Civil Eng 32(6):04018050
28. Raphael B, Smith FC (1998) Finding the right model for bridge diagnosis. Artificial intelligence in structural engineering. Springer, Berlin, pp 308–319
29. Sawyer JP, Rao SS (2000) Structural damage detection and identification using fuzzy logic. AIAA J 38(12):2328–2335
30. Schittkowski K (1986) NLPQL: a FORTRAN subroutine solving constrained nonlinear programming problems. Ann Oper Res 5(1):485–500
31. Schlune H, Plos M, Gylltoft K (2012) Safety formats for nonlinear analysis of concrete structures. Mag Concr Res 64(7):563–574
32. SIA 269 (2011) Existing structures—bases. Zurich, Switzerland
33. Sidak Z (1967) Rectangular confidence regions for the means of multivariate normal distributions. J Am Stat Assoc 62(318):626–633
34. Simoen E, Papadimitriou C, Lombaert G (2013) On prediction error correlation in bayesian model updating. J Sound Vib 332(18):4136–4152
35. Spencer J, Billie F, Cho S (2011) Wireless smart sensor technology for monitoring civil infrastructure: technological developments and full-scale applications. In: Proceedings of the World Congress on Advances in Structural Engineering and Mechanics (ASEM'11). Seoul, South Korea
36. SS EN 1991-2 Eurocode 1 (2012) Actions on structures—part 2: traffic loads on bridges. Building and Construction Standards Committee, Singapore
37. SS EN 1992-2 Eurocode 2 (2012) Design of concrete structures—concrete bridges—design and detailing rules. Building and Construction Standards Committee, Singapore
38. Tarantola A (2005) Inverse problem theory: methods for data fitting and parameter estimation. SIAM, Philadelphia
39. Tarantola A (2006) Popper, Bayes and the inverse problem. Nat Phys 2(8):492–494
40. Urbanski MK, Wasowski J (2003) Fuzzy approach to the theory of measurement inexactness. Measurement 34(1):67–74